HHS Public Access

Author manuscript

Dev Dyn. Author manuscript; available in PMC 2016 August 01.

Published in final edited form as:

Dev Dyn. 2015 August ; 244(8): 935–947. doi:10.1002/dvdy.24285.

The inorganic anatomy of the mammalian preimplantation embryo and the requirement of zinc during the first mitotic divisions

Betty Y. Kong[1,*], **Francesca E. Duncan**[1,*], **Emily L. Que**[2], **Yuanming Xu**[1], **Stefan Vogt**[3], **Thomas V. O'Halloran**[2,4,†], and **Teresa K. Woodruff**[1,4,†]

[1]Department of Obstetrics and Gynecology, Northwestern University, Feinberg School of Medicine, 250 East Superior Street, Suite 3-2303, Chicago, IL 60611

[2]Department of Chemistry, Northwestern University, 2145 Sheridan Road, Evanston, IL 60208

[3]X-ray Science Division, Argonne National Laboratory, Argonne, IL, USA

[4]Department of Molecular Biosciences, 2205 Tech Drive, Hogan 2-100, Evanston, IL 60208

Abstract

Background—Zinc is the most abundant transition metal in the mammalian oocyte, and dynamic fluxes in intracellular concentration are essential for regulating both meiotic progression and fertilization. Whether the defined pathways of zinc utilization in female meiosis directly translate to mitotic cells, including the mammalian preimplantation embryo, have not been studied previously.

Results—We determined that zinc is the most abundant transition metal in the preimplantation embryo, with levels an order of magnitude higher than those of iron or copper. Using a zinc-specific fluorescent probe, we demonstrated that labile zinc is distributed in vesicle-like structures in the cortex of cells at all stages of preimplantation embryo development. To test the importance of zinc during this period, we induced zinc insufficiency using the heavy metal chelator N,N,N′,N′-tetrakis-(2-pyridylmethyl)-ethylenediamine (TPEN). Incubation of embryos in media containing TPEN resulted in a developmental arrest that was specific to zinc chelation and associated with compromised mitotic parameters. The developmental arrest due to zinc insufficiency was associated with altered chromatin structure in the blastomere nuclei and decreased global transcription.

Conclusions—These results demonstrate for the first time that the preimplantation embryo requires tight zinc regulation and homeostasis for the initial mitotic divisions of life.

Keywords

Preimplantation embryo; zinc; mitosis

[†]Corresponding Authors: Teresa K. Woodruff, Ph.D., Department of Obstetrics and Gynecology, Northwestern University, 303 East Superior Street, Lurie 10-121, Chicago, IL 60611, Phone: 312-503-2503, Fax: 312-503-0219, tkw@northwestern.edu and Thomas V. O'Halloran, Ph.D., Department of Chemistry and Department of Molecular Biosciences, Northwestern University, 2145 Sheridan Road, Evanston, IL 60208, Phone: 847-491-5060, t-ohalloran@northwestern.edu.

[*]These authors contributed equally to the manuscript.

Introduction

There are two key transitions in mammalian development that are essential for giving rise to the next generation. The first is the transition of the prophase I-arrested, germinal vesicle (GV) intact oocyte into a fertilization-competent metaphase II-arrested (MII) egg through the process of meiotic maturation (reviewed in (Mehlmann, 2005)). The second is the transition of an MII egg into an embryo upon fertilization that divides by mitosis and relies on its own genome for subsequent embryo development (reviewed in (Zernicka-Goetz et al., 2009)). Recent *in vitro* and *in vivo* studies have demonstrated a profound requirement for zinc during female mammalian gamete development and fertilization, suggesting that this metal and its regulation have direct consequences on fertility (Kim et al., 2010; Suzuki et al., 2010; Bernhardt et al., 2012; Kong et al., 2012; Tian and Diaz, 2012; Zhao et al., 2014a).

Insight into zinc as a key inorganic regulator of the oocyte-to-egg transition and the egg-to-embryo-transition was first gleaned from synchrotron-based X-ray fluorescence microscopy (XFM) experiments, which allowed the precise determination of the total metal content of individual mammalian gametes and early embryos (Kim et al., 2010). Through these studies the striking observation was made that the oocyte's total zinc content is an order of magnitude larger than its total iron or copper contents, suggesting a specialized function for this transition metal during female meiosis. This is a departure from the ratios observed in most cell types, such as *Escherichia coli*, which have similar total zinc and iron levels and ten-fold lower copper levels (Outten and O'Halloran, 2001; Gilston, 2013). Additionally, the total zinc content undergoes dynamic fluxes, increasing significantly during meiotic maturation and decreasing at the time of fertilization (Kim et al., 2010). Zinc influx during meiosis is dependent on two zinc transporters, ZIP6 and ZIP10, whereas the physiologic decrease of zinc at fertilization occurs through a coordinated release of zinc from cortically-enriched vesicles in repetitive exocytic events termed "zinc sparks" (Kim et al., 2011; Kong et al., 2014; Que et al., 2014). Such changes in zinc levels are essential for proper meiotic progression and fertilization, and a key target of zinc dynamics during this period of early development is the meiotic cell cycle. Studies in which zinc levels have been manipulated genetically or chemically through zinc-specific chelators and ionophores have demonstrated that zinc regulation is required to maintain the prophase I and metaphase II arrests through interactions with cell cycle proteins including MOS, EMI2 and protein kinase C (Suzuki et al., 2010; Bernhardt et al., 2011; Tian and Diaz, 2011; Kong et al., 2012; Kong et al., 2014; Zhao et al., 2014b).

Although we have acquired a broad understanding of zinc biology during female meiosis and fertilization, correspondingly less is known about this transition metal during mammalian preimplantation embryo development. This period refers to the early stages of development that occur prior to embryo implantation into the uterus. Poised at the interface between meiosis and mitosis, the preimplantation embryo maintains significant maternal legacy while transforming into its own lineage (Tadros and Lipshitz, 2009). Preimplantation embryo development encompasses several critical events including: mitotic cleavage divisions to increase the embryo's cell number without increasing its size, zygotic genome activation during which the embryo becomes reliant on its own products of transcription and translation, compaction and cell polarization which define the outside and inside of the

embryo, and differentiation and lineage specification which distinguishes the embryo proper from extra-embryonic tissues (Zernicka-Goetz et al., 2009).

Several studies imply that there is a very sensitive requirement for zinc action and homeostasis during preimplantation embryo development. For example, zinc deficiency during pregnancy is associated with detrimental outcomes for embryo and fetal development (Apgar and Fitzgerald, 1985; Peters et al., 1991; Keen et al., 2003). Moreover, a mouse model of acute dietary zinc deficiency demonstrated that even short exposure to reduced zinc levels during the period of terminal oocyte maturation was sufficient to significantly disrupt preimplantation embryo development (Tian and Diaz, 2013). In contrast to these models of zinc insufficiency, metal supplementation of *in vitro* maturation and embryo culture media is associated with positive embryonic developmental outcomes in several species (Stephenson and Brackett, 1999; Gao et al., 2007). Despite these observations, the precise metal content of the mammalian preimplantation embryo and how it responds to alterations in environmental zinc content remains unknown. In this study, we used XFM to determine the elemental composition of individual cleavage stage preimplantation embryos and demonstrated that total zinc levels were significantly higher than iron or copper and remained constant in the early embryo. Disruption of intracellular metal homeostasis in cleavage stage embryos using the heavy metal chelator N,N,N′,N′-tetrakis-(2-pyridylmethyl)-ethylenediamine (TPEN) was zinc-specific and resulted in developmental arrest due in part to altered chromatin structure and global transcription. These results illustrate the importance of zinc regulation in the preimplantation embryo and the dramatic developmental consequences of zinc insufficiency during the very first mitotic divisions that define the formation of a new organism.

Results

Elemental analysis of mouse preimplantation embryos by synchrotron-based X-ray fluorescence microscopy

The total metal content of a cell can be divided into two populations: that which is tightly bound to biopolymers and that which is labile and accessible to chelating probes – the latter category includes metal ions that are loosely bound to intracellular ligands in compartments or free in the cytosol. We used synchrotron-based XFM to evaluate the total elemental composition and distribution of individual one- (1C), two- (2C), four- (4C) and eight-cell (8C) embryos derived *in vivo* from timed mating. This technique utilizes the unique X-ray emission spectra of each element to generate a quantitative elemental map of the sample. The map is integrated along the z-axis and displayed as a two-dimensional image with total element content presented in units of μg per cm^2 after calibrating with standards from the US National Institute of Standards and Technology (Figure 1A). The total number of atoms per embryo was calculated using the integrated data as described previously (Kim et al., 2010). As has been reported in the female gamete, zinc was the most abundant transition metal in the preimplantation embryo compared to iron and copper by an order of magnitude, leading us to test whether zinc continues to have an important role during this developmental period (Figure 1B, Table 1) (Kim et al., 2010).

In contrast to the rise in total zinc and copper levels that occurs during meiotic maturation, these transition metals both remained constant throughout early embryo development and were similar to the levels observed in the GV oocyte, suggesting the continued functional significance of this metal pool in the preimplantation embryo (Figure 1B) (Kim et al., 2010). Of note, iron levels did change during preimplantation embryo development, with a 50% increase occurring between the 4C and 8C stages (Figure 1B). While still an order of magnitude lower than total zinc levels, this initial rise in iron during early embryo development may imply emerging roles for this transition metal in the later stages of development.

Labile zinc pools are cortically distributed throughout the preimplantation embryo

Given the striking abundance of zinc relative to iron and copper in the cleavage stage preimplantation embryo, we focused our attention further on this transition metal. To distinguish the sub-cellular localization of labile zinc from total zinc during preimplantation embryo development, we performed live imaging with membrane permeant zinc-specific fluorophores (Figure 2). Staining with FluoZin-3 AM demonstrated that labile zinc localizes to discrete punctate structures in the preimplantation embryo (Figure 2A). These punctate structures have a cytoplasmic localization and are enriched at the cortex particularly during the early cleavage stages (Figure 2Aii′–iv′). This punctate and cortical staining pattern is reminiscent of what we described previously in the unfertilized metaphase II-arrested egg (MII egg), although the zinc punctae in the early embryo were not asymmetrically distributed as they were in the MII egg (Kim et al., 2011; Que et al., 2014).

The specificity of labile zinc distribution in the preimplantation embryo was confirmed using two approaches. First, use of a chemically distinct zinc fluorophore, ZincBY-1, revealed a punctate cytoplasmic staining pattern that was indistinguishable from that observed with FluoZin-3 AM (Figure 2Bi′). Second, addition of the chelator TPEN, which has high affinity for zinc, completely quenched the fluorescent signal, indicating that the observed fluorescence is zinc-specific and supporting the idea that labile zinc is compartmentalized (Figure 2Bii′, iv′).

Zinc insufficiency interferes with mitotic progression of the cleavage stage embryo

To determine the importance of zinc during precise stages of preimplantation embryo development, we perturbed zinc homeostasis using TPEN to limit intracellular zinc availability. As has been reported previously and in this study, TPEN exposure can reduce total and labile zinc populations in the mammalian oocyte and embryo (Figure 2B) (Kim et al., 2010). Specifically, we cultured 1C, 2C and 4C stage embryos in the presence or absence of either 1 μM or 10 μM TPEN for 24 h and monitored developmental progression by morphology (Figure 3). A significant developmental arrest was observed in embryos exposed to both 1 μM and 10 μM TPEN during culture compared to controls. This phenotype was dose dependent, as developmental arrest was more pronounced at the higher TPEN concentration (Figure 3). Only 21.3% (SEM ±10.6%) of 1C embryos cultured in 1 μM TPEN cleaved to the 2C stage or beyond, and 0.0% (SEM ±0%) of those in 10 μM TPEN progressed. In contrast, 96.4% (SEM ±1.5%) of control 1C embryos cleaved (Figure 3A). Similarly, TPEN treatment of 2C stage embryos also caused significant developmental

arrest: only 40.0% (SEM ±6.6%) of those cultured in 1 μM TPEN and 16.7% (SEM ±10.%) of those cultured in 10 μM TPEN progressed to the 4–8C stage after 24h compared to 90.9% (SEM ±3.7%) of control embryos (Figure 3B). Finally, of cultured 4C embryos, 13.1% (SEM ±7.0%) of those treated with 1 μM TPEN and 6.02% (SEM ±4.2%) of those treated with 10 μM TPEN progressed to or beyond the 8C stage (Figure 3B). In contrast, 94.2% (SEM ±2.6%) of 4C embryos cultured in control medium progressed to form 8C embryos, morulae or early blastocysts (Figure 3C). Given the significant percentage of arrest phenotypes observed at TPEN concentrations as low as 1 μM, all further zinc chelation experiments were performed using this lower TPEN concentration. The arrest induced by culture in 1 μM TPEN medium was irreversible, as two-cell embryos placed back in normal culture medium after the 24h TPEN incubation remained arrested at the two-cell stage (data not shown). Interestingly, treatment of mouse oocytes with TPEN concentrations less than 10 μM TPEN did not result in any phenotypic abnormalities or impact meiotic progression (Kim et al., 2010).

The affinity of TPEN for chelating copper is higher than its affinity for zinc, and thus it was possible that the observed cleavage arrests were due to effects on copper and not zinc. To determine whether the TPEN effect on embryo development was specifically due to zinc chelation, we cultured 1C, 2C, and 4C embryos for 24 h in the presence of two different copper-specific chelators, neocuproine or ammonium tetrathiomolybdate (TM), and monitored developmental progression (Figure 4). Compared to culture in 1 μM TPEN, which we demonstrated causes a significant developmental arrest, culture in the presence of 1 μM neocuproine or 1 μM TM had no effect on cleavage divisions at any stage of development (Figure 4, Table 2), suggesting the phenotypes observed of TPEN chelation result from perturbation of zinc homeostasis, and not copper. These results are further confirmed by the rescue of normal development by culturing embryos in the presence of TPEN and zinc, similar to what has been previously reported during oocyte maturation (data not shown, (Kim et al., 2010; Kong et al., 2012)).

Because our analysis of embryo development in the presence of zinc and copper chelators was thus far limited to morphological assessment, we next performed a more in depth quantitative characterization using markers of mitotic division, including blastomere number, mitotic index and midbody number (Figure 5; Table 3). This type of analysis was particularly important during the later cleavage stages where it can be difficult to accurately assess blastomere number by transmitted light microscopy. We found that culture of 2C or 4C embryos in the presence of TPEN caused a reduction in all mitotic parameters examined (Figure 5B–D, F–H). For example, 2C embryos cultured in 1 μM TPEN had an average of 3.2 blastomeres/embryo (SEM ±0.14), a mitotic index of 0.018 (SEM ±0.012), and 1.0 midbodies/embryo (SEM ±0.13). These values were all less than those measured in embryos cultured in control media or in the presence of copper chelators (Figure 5B–D). The impact of zinc chelation on mitotic parameters was even more pronounced when 4C embryos were cultured in 1 μM TPEN (Figure 5F–H). 4C embryos cultured in control media had 18.7 blastomeres/embryo (SEM ±0.015), a mitotic index of 0.061 (SEM ±1.3) mitotic blastomeres/embryo, and 6.5 (SEM ±0.87) midbodies/embryo. These parameters were all significantly less – 7.8 (SEM ±0.48), 0.0 (SEM ±0.0), 0.67 (SEM ±0.27), respectively - in the same cohort of embryos cultured in TPEN. In contrast, parameters for embryos cultured

in copper chelators were not statistically different compared to control. Taken together, these results demonstrate that the preimplantation embryo is exquisitely sensitive to changes in metal homeostasis and provide strong support for the zinc-specificity of the observed developmental arrest.

TPEN-induced zinc insufficiency alters chromatin configuration and global transcription

When analyzing the mitotic parameters of embryos cultured in zinc and copper chelators, we observed that there were striking differences in chromatin configuration between treatment groups (Figure 6A). In 94.1% (SEM ±0.064%), 95.2% (SEM ±0.38%), and 93.9% (SEM ±2.7%) of 2C embryos cultured in KSOM alone, with neocuproine, or with TM, respectively, the blastomere nuclei exhibited a euchromatin configuration with loosely packed DNA surrounding the nucleolus (Figure 6A, B, Table 4). This was in contrast to 2C embryos cultured in 1 μM TPEN in which only 13.2% (SEM ±0.90%) had nuclei with this type of chromatin configuration. Instead 86.2% (SEM ±1.5%) of TPEN-treated embryos had nuclei with a heterochromatin configuration, in which the DNA was tightly packed around the periphery of the nucleus (Figure 6A, B). This heterochromatin configuration was observed in TPEN-treated embryos that remained arrested at the 2C stage as well as those that were able to progress to the 4C stage (Figure 6B). However, the heterochromatin phenotype was much more pronounced in the embryos that remain arrested at the 2C stage, suggesting that this chromatin configuration may underlie the developmental arrest (Figure 6A).

Chromatin configuration is highly coordinated with transcriptional activity. For example, fully-grown oocytes are transcriptionally quiescent, and this quiescence is associated with a defined nucleolar architecture referred to as surrounded nucleolus, in which heterochromatin is tightly compacted around the nucleolus (Bouniol-Baly et al., 1999; Inoue et al., 2008). Given the similarity in chromatin configuration between transcriptionally quiescent oocytes and the blastomeres of TPEN-treated embryos, we were interested in determining how TPEN affected global transcription in the cleavage stage embryo. Global transcription was quantified using a transcriptional assay that detects the incorporation of 5-ethynyl uridine (5EU) into newly synthesized RNA (Jao and Salic, 2008). We compared 5EU incorporation between nuclei of TPEN-treated embryos arrested at the 2C stage to those of control 2C embryos that were cultured from the 1C stage (Figure 6C, D). We observed a significant decrease of over 80% in 5EU incorporation following exposure to TPEN (2.2 pixel intensity units, SEM ±0.64) compared to controls (12 pixel intensity units, SEM ±1.4), indicating a global disruption of transcription in TPEN treated embryos (Figure 6D). These findings provide mechanistic insight into how zinc insufficiency may be mediating developmental arrest, as transcription inhibition is known to inhibit zygotic genome activation and cause cleavage arrest at the 2C stage (Aoki et al., 1997).

Discussion

The developmental capacity of the preimplantation mammalian embryo relies largely on the quality of the female gamete. Before the activation of the embryonic genome at the 2C stage in mouse development, the early embryo is solely dependent on the egg for survival, with

minimal contribution from the stored organelles and macromolecules of the sperm (Sutovsky and Schatten, 2000; Lee et al., 2014). Zinc is an important factor in the proper development of the oocyte through meiotic maturation and egg activation, and here we have extended our knowledge of zinc physiology in the female gamete to its function during preimplantation embryo development (Kim et al., 2010; Bernhardt et al., 2012; Kong et al., 2012; Tian and Diaz, 2012).

Using quantitative elemental analysis, which captures a two-dimensional representation of total metal content, we report for the first time the relationships between zinc, copper and iron content in early embryogenesis. These results coupled with the extreme sensitivity of embryos to zinc chelation tell a valuable story and help establish that the zinc requirements of the mitotic cell cycle are quite different from those reported in the meiotic stages just a few hours earlier in development. Whether this difference in zinc requirement is unique to the preimplantation embryo or more broadly applicable to all mitotic cells remains an area of investigation. Moreover, using two zinc-responsive dyes with differing properties, we captured optical sections through the embryo and highlight that labile zinc is distributed in vesicle-like structures throughout the cytoplasm of the embryo, but are particularly enriched in the cortical region. The XRF measurements were made at low spatial (ca 400nm) resolution and thus do not shed light on possible vesicular distributions. However, there is strong precedence for zinc localization to vesicles in both mouse and human gametes (Kim et al., 2011; Kong et al., 2014). In the case of mouse MII eggs, a number of physical methods have shown that on average one million zinc atoms are loaded into vesicles with an average diameter of 250 nm in diameter (Que et al., 2014). We recently demonstrated that two maternally-derived zinc transporters are present in the ooplasmic membrane, ZIP6 and ZIP10. They mediate zinc uptake during meiotic progression and also have a cortical localization that persists throughout preimplantation embryo development (Kong et al., 2014). Future studies are warranted to determine whether these transporters or ones that have a zygotic pattern of gene expression (ZNT1, ZNT4, or ZNT5) are essential during this window of development (Kong et al., 2014).

Interestingly, in contrast to zinc or copper, iron levels increased significantly at the eight-cell embryo stage. One explanation for this rise is the role of this transition metal in mitochondrial function during aerobic respiration. Mitochondria are largely dormant in the oocyte and early embryo, as mitochondrial respiration accounts for less than 10% of glucose metabolism but dramatically rises to 85% in the blastocyst (Bavister and Squirrell, 2000). Further, the compaction of mitochondrial cristae, the initiation of mitochondrial replication and an increase in the utilization of glucose all occur at the blastocyst stage (Houghton and Leese, 2004). Thus, the increase in total iron abundance at the eight-cell stage parallels its functional utilization in the upcoming developmental stages and may be indicative of the embryo's transition toward a more somatic cell-like inorganic signature, in which the concentrations of zinc and iron are more similar to each other and both greater than copper (Suhy et al., 1999; Outten and O'Halloran, 2001). The mechanism and significance of this increase in intracellular iron at the 8C stage at a time when mitochondria biogenesis is beginning will be pursued in future years.

To determine how the early embryo responds to changes in environmental metal content, we cultured embryos in the presence of the heavy metal chelator, TPEN. As has been observed in the oocyte, this chelator specifically decreased intracellular populations of zinc in the embryo (Kim et al., 2010). When zinc insufficiency was induced at any point during the first three mitotic divisions, developmental progression was compromised. Of note, we observed significant arrest in development when preimplantation embryos were exposed to 1 μM TPEN. This concentration of TPEN is 10-fold less than the minimum TPEN concentration required to elicit distinct meiotic cell cycle defects in the oocyte (Kim et al., 2010; Bernhardt et al., 2012; Kong et al., 2012). It is also significantly less than the TPEN concentrations (20–50 μM) used to induce apoptosis in somatic cells, including thymocytes, lymphocytes, keratinocytes and HeLa cells (Zalewski et al., 1993; Treves et al., 1994; Parat et al., 1997; Chimienti et al., 2001). These results imply that the preimplantation embryo is more sensitive to perturbations in metal homeostasis than the unfertilized gamete or other somatic cells. In addition, not all stages of preimplantation embryo development were equally responsive to changes in zinc. For example, a significant disruption of the plasma membrane was observed in 1C embryos cultured in the presence of even 1 μM TPEN, but this was never observed in 2C or 4C embryo cultures at this chelator concentration (Figure 4G). Of note, blastocyst stage embryos were the most sensitive to zinc chelation, exhibiting significant changes in morphology at 0.5 μM TPEN (data not shown). These findings undoubtedly have clinical ramifications, as the egg to embryo transition traverses the entire female reproductive system, from the ovarian follicle through the oviduct and into the uterus. Slight alterations in zinc availability in any of these environments, whether through physiological changes or assisted reproductive technologies, may have profound consequences on the success of a fertilization event that gives rise to a healthy offspring. In particular, it would be of great interest to determine whether differences in metal content exist between embryos derived from in vitro fertilization and natural mating, as this could potentially be applied to a clinical setting as a marker of embryo quality.

Our results suggest that zinc insufficiency during early embryo development has a direct or indirect effect on cell cycle progression because TPEN exposure resulted in a reduction in several mitotic parameters including blastomere number, mitotic index, and midbody number. A direct effect on the cell cycle may involve the protein Early Mitotic Inhibitor 1 (EMI1). EMI1 is the mitotic homolog of EMI2, an Anaphase Promoting Complex (APC/C) inhibitor that regulates the meiosis I to meiosis II transition and is a major target of zinc activity during meiosis (Suzuki et al., 2010; Bernhardt et al., 2012). Similar to EMI2, EMI1 also contains a highly conserved zinc-binding region and is known to require zinc for proper function. EMI1 is required for early embryogenesis, as the knockout mouse is embryonic lethal due to a defect in mitotic progression during preimplantation embryo development (Lee et al., 2006). These data raise the distinct possibility that zinc insufficiency prevents the proper functioning of EMI1 during embryonic divisions, and thus disrupts the blastomeres from progressing through mitosis.

Zinc insufficiency may also indirectly impact the mitotic cell cycle in the preimplantation embryo development via disruption of gene transcription, which was observed in response to TPEN exposure. In the mouse, the zygotic genome of the early embryo remains largely quiescent until the 2C stage, at which point the maternal-to-zygotic transition (MZT) takes

place, marking a dramatic shift in transcriptional activity (Zeng and Schultz, 2005; Tadros and Lipshitz, 2009). There is a targeted degradation of maternal RNA and proteins that had previously supported embryonic growth accompanied by a dramatic increase in the biosynthesis of genes from the newly recombined embryonic genome (Flach et al., 1982). If the zygotic genome does not activate, embryo development past the early cleavage stages is severely compromised (Li et al., 2010). Thus, the observed block in preimplantation embryo development in response to zinc chelation may occur in part because of transcriptional inhibition. Such a mechanism is likely given that zinc-binding proteins comprise up to 10% of the eukaryotic proteome and that zinc is an essential cofactor for many transcriptional regulators and polymerases (Andreini et al., 2006a; Andreini et al., 2006b; Fukada et al., 2011). Whether the developmental arrest we observed is due to failure of global zygotic genome activation or to lack of specific gene expression remains to be determined.

The results reported in this manuscript extend our knowledge of inorganic physiology from the GV stage oocyte all the way to the 8C stage embryo. A further continuation of this work into the later stages of embryo development, including blastocyst formation and implantation, is ongoing. Having data on this broader temporal time frame of development not only allows us to gain insight into the important role of zinc across the meiotic-mitotic transition, but also allows us to appreciate the truly unique and complex events of the egg-to-embryo transition. The presence of high total zinc levels compared to iron or copper in the preimplantation embryo suggests a continued role for this transition metal in regulating the developmental potential of the early embryo. Indeed, disruption of zinc homeostasis resulted in significant developmental arrest, a reduction in several mitotic parameters, and a profound decrease in overall transcriptional activity. Overall, our studies implicate the presence of zinc regulation in the control of the cell cycle, both meiotic and mitotic. However, unlike the transcriptionally quiescent mature oocyte, the early embryo takes on a very active state as it prepares the zygotic machinery necessary to sustain the rest of development. Thus, it is possible that multiple zinc-dependent pathways, including both specific cell cycle regulators and broad transcriptional mechanisms, may be simultaneously impacted during this next stage of development in the egg-to-embryo transition.

Experimental Procedures

Animals

All experiments were performed using CD-1 mice (Harlan Laboratories) in accordance with the National Institutes of Health Guide for the Care and Use of Laboratory Animals and under protocols approved by the Northwestern University Institutional Animal Care and Use Committee (IACUC). Mice were housed and bred in a controlled barrier facility in the Center for Comparative Medicine at Northwestern University (Chicago, IL). Food and water were provided ad libitum. Temperature, humidity and photoperiod (14L:10D) were kept constant.

Embryo collection and culture

Embryos were collected from adult CD1 female mice 6–8 weeks old after superovulation and timed mating. Female mice were injected intraperitonealy with 5 IU pregnant mare

serum gonadotropin (PMSG; Calbiochem, La Jolla, CA), and 46–48 hr later with 5 IU human chorionic gonadotropin (hCG; Sigma-Aldrich, St. Louis, MO). Following hCG injection females were mated with male CD1 mice (>10 weeks old). A maximum of two females were housed per individual male. 1C, 2C, 4C, and 8C embryos were collected from the ampullae or flushed from the oviducts at 18–20 h, 38–42 h, 60–62,h or 66 h post-hCG, respectively. All embryo culture was done at 37°C and 5% CO_2 in air in potassium simplex optimized medium (KSOM; Millipore, Billerica, MA). For chelator experiments, embryos were cultured for 24 h in KSOM supplemented with tetrakis-(2-pyridylmethyl)ethylenediamine (TPEN; 1 μM or 10 μM), neocuproine (1 μM), or TM (1 μM). All chelators were from Sigma-Aldrich. Control embryos were cultured in media alone. Following culture, the number of embryos at each stage of development were scored by light microscopy.

TPEN is a heavy metal chelator that binds a variety of metals with high affinity including Zn(II) (LogKa = 18.0), Cu(II) (LogKa = 20.6), and Fe(II) (LogKa = 14.6) (Martell, 1977; Arslan et al., 1985). Tetrathiomolybdate binds Cu(I) (LogKa = 8) selectively over other biological metal ions including Ca(II), Fe(II), Mg(II), and Zn(II) (Juarez et al., 2006). This compound has the ability to bind copper in protein active sites (Alvarez et al., 2010). Neocuproine forms strong 2:1 complexes with Cu(I) ($Log\beta_2$ = 19.5), but has weaker affinity for Cu(II) ($Log\beta_1$ = 5.2, $Log\beta_2$ = 11.0) and Zn(II) ($Log\beta_1$ = 4.1, $Log\beta_2$ = 7.7) (Irving, 1962; Hawkins, 1963).

Synchrotron-based X-ray fluorescence microscopy

1C, 2C, 4C, and 8C embryos were prepared for XFM as previously described for oocytes (Kim et al., 2010). Briefly, embryos were transferred from culture medium to a 5 mm X 5 mm silicon nitride window (Silson, England). To wash away salts transferred with the samples, the windows were flushed with 100 mM ammonium acetate solution several times under a dissection microscope and allowed to dehydrate. This left the morphology of the sample largely intact without causing membrane rupture.

XFM was performed at the Advanced Photon Source (Argonne National Laboratory) on Beamline 2-ID-E. Ten keV X-rays were monochromatized and focused to a spot size of 0.5 μm × 0.6 μm using Fresnel-zone plate optics (X-radia). Scans were done in steps of 2 μm and fluorescence spectra were collected with a 1 second dwell time using a silicon drift detector (Vortex-EM). Flyscans were taken with 0.5 μm pixel size and a dwell time of 50 ms. Image processing and quantification were performed with MAPS software. Using thin-film standards NBS-1832 and NBS-1833 (US National Bureau of Standards), the fluorescence signal was converted to a two-dimensional concentration in μg per cm^2, which was then converted to atom number using the atomic weight for each element and Avogadro's number. To determine total elemental content of various stage embryos, regions of interest were designated on the two-dimensional images and analyzed using ImageJ software (U.S. National Institutes of Health, Bethesda, MD). It was assumed that no elemental content was lost during sample preparation.

Labile zinc imaging

Live cell imaging was done to detect labile zinc in preimplantation embryos using two zinc-specific fluorophores: FluoZin-3 AM (Invitrogen, Carlsbad, CA) and ZincBY-1 (Que et al., 2014). FluoZin3-AM has a K_d = 15 nM and is highly specific for Zn(II) (Gee et al., 2002). ZincBY-1 is a newly synthesized fluorescent probe for zinc, and detailed information on its synthesis and properties can be found in (Que et al., 2014). In brief, it has a K_d = 2.5 nM and is selective for Zn(II) over a range of other biological metals, including Ca^{2+}, Na^{+}, K^{+}, Fe^{2+}, and Fe^{3+}. FluoZin3-AM was prepared as a 10 mM stock solution in DMSO and diluted 1:1000 in KSOM for staining of embryos. ZincBY-1 was prepared as a 50 μM stock solution in DMSO and diluted 1:1000 in KSOM. Embryos were either incubated in 10 μM FluoZin-3 AM or 50 nM ZIncBY-1 for 30 min. To confirm the zinc specificity of fluorescent staining, embryos were then incubated in 10 μM TPEN for 10 minutes (for ZincBY-1) or 50 μM TPEN for 30 minutes (for FluoZin3-AM) after the initial imaging and then re-imaged. All embryos were imaged in drops of KSOM overlaid with embryo culture oil (Irvine Scientific) in glass-bottom dishes (Bioptechs Inc, Butler, PA). Images were acquired as Z-stacks with a 1 μm step size on a TCS SP5 inverted laser-scanning confocal microscope (Leica Microsystems, Bannockburn, IL) equipped with a stage top incubator (Tokai Hit, Japan), 40× oil-immersion objective, and HeNe (543 nm), Ar (488 nm) and near-UV (405 nm) laser lines. Images were processed using LAS AF (Leica Microsystems) and ImageJ.

Immunofluorescence and Microscopy

The cytoskeleton morphology and chromatin configuration of 2C and 4C embryos cultured in the presence or absence of metal chelators were examined using whole mount immunofluorescence methods and confocal microscopy. Except where otherwise specified, steps in this protocol were performed at room temperature. Eggs were fixed in 3.8% paraformaldehyde (PFA, Electron Microscopy Sciences, Hatfield, PA) supplemented with 0.1% Triton X-100 (Sigma-Aldrich, St. Louis, MO) for 1.5 h at 37°C. Embryos were then permeabilized in PBS containing 0.1% Triton X-100 and 0.3% bovine serum albumin (BSA; MP Biomedicals, Solon, OH) for 15 min and blocked in blocking solution (PBS containing 0.01% Tween-20 (Sigma-Aldrich) and 0.3% BSA). Embryos were incubated in Alexa Fluor 488-conjugated α-tubulin antibody (1:100; Cell Signaling Technologies) and rhodamine-phalloidin (1:50; Invitrogen) diluted in blocking solution overnight at 4°C to visualize the microtubule and actin cytoskeletons, respectively. Embryos were washed in blocking solution and then mounted in Vectashield with 4(6-diamidino-2-phenylindole) (DAPI; Vector Laboratories Inc., Burlingame, CA). Images were acquired as Z-stacks with a 1 μm step size on the confocal microscope as described above and processed on ImageJ software.

Optical sections for each embryo were analyzed to assess parameters including blastomere and midbody number, mitotic index, and chromatin configuration. The number of blastomeres per embryo was determined based on the number of DAPI-positive nuclei. Chromatin configuration was classified as euchromatin or heterochromatin based on the pattern of DAPI staining (Bouniol-Baly et al., 1999). The mitotic index was calculated as the number of blastomeres in metaphase or anaphase (as evidenced by the DNA configuration and presence of a mitotic spindle) divided by the total number of blastomeres in the embryo. The number of midbodies was determined based on the number of α-tubulin-enriched

structures connecting individual blastomeres. See Figures 5A, E and Figure 6A for representative images of these parameters.

5-ethynyl uridine (5EU) transcriptional assay

We assessed global transcription using the Click-iT RNA Alexa Fluor 488 Imaging Kit according to the manufacturer's instructions (Invitrogen). Briefly, embryos cultured in the presence or absence of chelators were incubated in 4 mM EU in KSOM for 100 mins at 37°C. Embryos were then fixed in 3.8% PFA for 1 h at room temperature, and washed and blocked as described above. After rinsing with blocking buffer, the embryos were incubated in the Click-iT cocktail according to the manufacturer's instructions using a 1:250 dilution of Alexa Fluor 488-conjugated azide for 30 mins at room temperature. Stained embryos were washed in blocking solution, mounted in Vectashield containing DAPI and imaged by confocal microscopy as described above. The mean intensity of the nuclear area was quantified using LAS AF software by selecting the region of interest (ROI) in the 5EU channel and corrected for background.

Statistical Analysis

Elemental concentrations and embryo parameters were analyzed for statistical significance using one-way ANOVA with Bonferroni post-hoc test. All statistical tests were performed using the software Prism 4.0 (GraphPad Software, San Diego, CA). $p < 0.05$ was considered statistically significant.

Acknowledgments

Grant sponsor: This work was supported by the National Institutes of Health (P01 HD021921 and GM038784) and a Medical Research Award from the W. M. Keck Foundation.

The authors wish to acknowledge Dr. Miranda Bernhardt and Dr. Alison Kim for useful discussions and Jennifer Pahnke and Alexander Gunn for their technical assistance. This research used resources of the Advanced Photon Source, a U.S. Department of Energy (DOE) Office of Science User Facility operated for the DOE Office of Science by Argonne National Laboratory under Contract No. DE-AC02-06CH11357. This work was supported by the National Institutes of Health (P01 HD021921) and a Medical Research Award from the W. M. Keck Foundation.

References

Aiken CE, Swoboda PP, Skepper JN, Johnson MH. The direct measurement of embryogenic volume and nucleo-cytoplasmic ratio during mouse pre-implantation development. Reproduction. 2004; 128:527–535. [PubMed: 15509698]

Alvarez HM, Xue Y, Robinson CD, Canalizo-Hernandez MA, Marvin RG, Kelly RA, Mondragon A, Penner-Hahn JE, O'Halloran TV. Tetrathiomolybdate inhibits copper trafficking proteins through metal cluster formation. Science. 2010; 327:331–334. [PubMed: 19965379]

Andreini C, Banci L, Bertini I, Rosato A. Counting the zinc-proteins encoded in the human genome. J Proteome Res. 2006a; 5:196–201. [PubMed: 16396512]

Andreini C, Banci L, Bertini I, Rosato A. Zinc through the three domains of life. J Proteome Res. 2006b; 5:3173–3178. [PubMed: 17081069]

Aoki F, Worrad DM, Schultz RM. Regulation of transcriptional activity during the first and second cell cycles in the preimplantation mouse embryo. Dev Biol. 1997; 181:296–307. [PubMed: 9013938]

Apgar J, Fitzgerald JA. Effect on the ewe and lamb of low zinc intake throughout pregnancy. J Anim Sci. 1985; 60:1530–1538. [PubMed: 4019343]

Arslan P, Di Virgilio F, Beltrame M, Tsien RY, Pozzan T. Cytosolic Ca2+ homeostasis in Ehrlich and Yoshida carcinomas. A new, membrane-permeant chelator of heavy metals reveals that these ascites tumor cell lines have normal cytosolic free Ca2+ J Biol Chem. 1985; 260:2719–2727. [PubMed: 3919006]

Bavister BD, Squirrell JM. Mitochondrial distribution and function in oocytes and early embryos. Hum Reprod. 2000; 15(Suppl 2):189–198. [PubMed: 11041524]

Bernhardt ML, Kim AM, O'Halloran TV, Woodruff TK. Zinc Requirement During Meiosis I-Meiosis II Transition in Mouse Oocytes Is Independent of the MOS-MAPK Pathway. Biology of Reproduction. 2011; 84:526–536. [PubMed: 21076080]

Bernhardt ML, Kong BY, Kim AM, O'Halloran TV, Woodruff TK. A zinc-dependent mechanism regulates meiotic progression in mammalian oocytes. Biology of Reproduction. 2012; 86:114. [PubMed: 22302686]

Bouniol-Baly C, Hamraoui L, Guibert J, Beaujean N, Szollosi MS, Debey P. Differential transcriptional activity associated with chromatin configuration in fully grown mouse germinal vesicle oocytes. Biology of Reproduction. 1999; 60:580–587. [PubMed: 10026102]

Chimienti F, Seve M, Richard S, Mathieu J, Favier A. Role of cellular zinc in programmed cell death: temporal relationship between zinc depletion, activation of caspases, and cleavage of Sp family transcription factors. Biochem Pharmacol. 2001; 62:51–62. [PubMed: 11377396]

Flach G, Johnson MH, Braude PR, Taylor RA, Bolton VN. The transition from maternal to embryonic control in the 2-cell mouse embryo. EMBO J. 1982; 1:681–686. [PubMed: 7188357]

Fukada T, Yamasaki S, Nishida K, Murakami M, Hirano T. Zinc homeostasis and signaling in health and diseases: Zinc signaling. Journal of biological inorganic chemistry : JBIC : a publication of the Society of Biological Inorganic Chemistry. 2011; 16:1123–1134. [PubMed: 21660546]

Gao G, Yi J, Zhang M, Xiong J, Geng L, Mu C, Yang L. Effects of iron and copper in culture medium on bovine oocyte maturation, preimplantation embryo development, and apoptosis of blastocysts in vitro. The Journal of reproduction and development. 2007; 53:777–784. [PubMed: 17420621]

Gee KR, Zhou ZL, Qian WJ, Kennedy R. Detection and imaging of zinc secretion from pancreatic beta-cells using a new fluorescent zinc indicator. J Am Chem Soc. 2002; 124:776–778. [PubMed: 11817952]

Gilston BA, OH TV. Metals in Cells: Control of Cellular Metal Concentration. Encyclopedia of Inorganic and Bioinorganic Chemistry. 2013:1–12.

Hawkins, CJaP; DD. Oxidation–reduction potentials of metal complexes in water. Part II. Copper complexes with 2,9-dimethyl- and 2-chloro-1,10-phenanthroline. J Chem Soc. 1963:2996–3002.

Houghton FD, Leese HJ. Metabolism and developmental competence of the preimplantation embryo. Eur J Obstet Gynecol Reprod Biol. 2004; 115(Suppl 1):S92–96. [PubMed: 15196724]

Inoue A, Nakajima R, Nagata M, Aoki F. Contribution of the oocyte nucleus and cytoplasm to the determination of meiotic and developmental competence in mice. Hum Reprod. 2008; 23:1377–1384. [PubMed: 18367455]

Irving H, Mellor DH. The stability of metal complexes of 1, 10-phenanthroline and its analogues. Part II. 2-Methyl- and 2,9-dimethyl-phenanthroline. J Chem Soc. 1962:5237–5245.

Jao CY, Salic A. Exploring RNA transcription and turnover in vivo by using click chemistry. Proc Natl Acad Sci U S A. 2008; 105:15779–15784. [PubMed: 18840688]

Juarez JC, Betancourt O Jr, Pirie-Shepherd SR, Guan X, Price ML, Shaw DE, Mazar AP, Donate F. Copper binding by tetrathiomolybdate attenuates angiogenesis and tumor cell proliferation through the inhibition of superoxide dismutase 1. Clin Cancer Res. 2006; 12:4974–4982. [PubMed: 16914587]

Keen CL, Hanna LA, Lanoue L, Uriu-Adams JY, Rucker RB, Clegg MS. Developmental consequences of trace mineral deficiencies in rodents: acute and long-term effects. The Journal of nutrition. 2003; 133:1477S–1480S. [PubMed: 12730447]

Kim AM, Bernhardt ML, Kong BY, Ahn RW, Vogt S, Woodruff TK, O'Halloran TV. Zinc Sparks Are Triggered by Fertilization and Facilitate Cell Cycle Resumption in Mammalian Eggs. ACS chemical biology. 2011; 6:716–723. [PubMed: 21526836]

Kim AM, Vogt S, O'Halloran TV, Woodruff TK. Zinc availability regulates exit from meiosis in maturing mammalian oocytes. Nature chemical biology. 2010; 6:674–681. [PubMed: 20693991]

Kong BY, Bernhardt ML, Kim AM, O'Halloran TV, Woodruff TK. Zinc Maintains Prophase I Arrest in Mouse Oocytes Through Regulation of the MOS-MAPK Pathway. Biology of reproduction. 2012; 87:11. [PubMed: 22539682]

Kong BY, Duncan FE, Que EL, Kim AM, TV OO, Woodruff TK. Maternally-derived zinc transporters ZIP6 and ZIP10 drive the mammalian oocyte-to-egg transition. Mol Hum Reprod. 2014

Lee H, Lee DJ, Oh SP, Park HD, Nam HH, Kim JM, Lim DS. Mouse emi1 has an essential function in mitotic progression during early embryogenesis. Molecular and Cellular Biology. 2006; 26:5373–5381. [PubMed: 16809773]

Lee MT, Bonneau AR, Giraldez AJ. Zygotic Genome Activation During the Maternal-to-Zygotic Transition. Annu Rev Cell Dev Biol. 2014; 30:581–613. [PubMed: 25150012]

Li L, Zheng P, Dean J. Maternal control of early mouse development. Development. 2010; 137:859–870. [PubMed: 20179092]

Martell, AE.; Smith, RM. Critical Stability Constants. New York: Plenum Press; 1977.

Mehlmann LM. Stops and starts in mammalian oocytes: recent advances in understanding the regulation of meiotic arrest and oocyte maturation. Reproduction. 2005; 130:791–799. [PubMed: 16322539]

Outten CE, O'Halloran TV. Femtomolar sensitivity of metalloregulatory proteins controlling zinc homeostasis. Science. 2001; 292:2488–2492. [PubMed: 11397910]

Parat MO, Richard MJ, Pollet S, Hadjur C, Favier A, Beani JC. Zinc and DNA fragmentation in keratinocyte apoptosis: its inhibitory effect in UVB irradiated cells. J Photochem Photobiol B. 1997; 37:101–106. [PubMed: 9043099]

Peters JM, Wiley LM, Zidenberg-Cherr S, Keen CL. Influence of short-term maternal zinc deficiency on the in vitro development of preimplantation mouse embryos. Proc Soc Exp Biol Med. 1991; 198:561–568. [PubMed: 1891470]

Que EL, Bleher R, Duncan FE, Kong BY, Gleber SC, Vogt S, Chen S, Garwin SA, Bayer AR, Dravid VP, Woodruff TK, O'Halloran TV. Quantitative mapping of zinc fluxes in the mammalian egg reveals the origin of fertilization-induced zinc sparks. Nat Chem. 2014 advance online publication.

Stephenson JL, Brackett BG. Influences of zinc on fertilisation and development of bovine oocytes in vitro. Zygote. 1999; 7:195–201. [PubMed: 10533702]

Suhy DA, Simon KD, Linzer DI, O'Halloran TV. Metallothionein is part of a zinc-scavenging mechanism for cell survival under conditions of extreme zinc deprivation. The Journal of biological chemistry. 1999; 274:9183–9192. [PubMed: 10092590]

Sutovsky P, Schatten G. Paternal contributions to the mammalian zygote: fertilization after sperm-egg fusion. Int Rev Cytol. 2000; 195:1–65. [PubMed: 10603574]

Suzuki T, Yoshida N, Suzuki E, Okuda E, Perry ACF. Full-term mouse development by abolishing Zn2+-dependent metaphase II arrest without Ca2+ release. Development. 2010; 137:2659–2669. [PubMed: 20591924]

Tadros W, Lipshitz HD. The maternal-to-zygotic transition: a play in two acts. Development (Cambridge, England). 2009; 136:3033–3042.

Tian X, Diaz FJ. Zinc Depletion Causes Multiple Defects in Ovarian Function during the Periovulatory Period in Mice. Endocrinology. 2011

Tian X, Diaz FJ. Zinc depletion causes multiple defects in ovarian function during the periovulatory period in mice. Endocrinology. 2012; 153:873–886. [PubMed: 22147014]

Tian X, Diaz FJ. Acute dietary zinc deficiency before conception compromises oocyte epigenetic programming and disrupts embryonic development. Dev Biol. 2013; 376:51–61. [PubMed: 23348678]

Treves S, Trentini PL, Ascanelli M, Bucci G, Di Virgilio F. Apoptosis is dependent on intracellular zinc and independent of intracellular calcium in lymphocytes. Exp Cell Res. 1994; 211:339–343. [PubMed: 8143781]

Zalewski PD, Forbes IJ, Betts WH. Correlation of apoptosis with change in intracellular labile Zn(II) using zinquin [(2-methyl-8-p-toluenesulphonamido-6-quinolyloxy)acetic acid], a new specific fluorescent probe for Zn(II). Biochem J. 1993; 296(Pt 2):403–408. [PubMed: 8257431]

Zeng F, Schultz RM. RNA transcript profiling during zygotic gene activation in the preimplantation mouse embryo. Dev Biol. 2005; 283:40–57. [PubMed: 15975430]

Zernicka-Goetz M, Morris SA, Bruce AW. Making a firm decision: multifaceted regulation of cell fate in the early mouse embryo. Nat Rev Genet. 2009; 10:467–477. [PubMed: 19536196]

Zhao MH, Kim NH, Cui XS. Zinc depletion activates porcine metaphase II oocytes independently of the protein kinase C pathway. In Vitro Cell Dev Biol Anim. 2014a

Zhao MH, Kwon JW, Liang S, Kim SH, Li YH, Oh JS, Kim NH, Cui XS. Zinc regulates meiotic resumption in porcine oocytes via a protein kinase C-related pathway. PLoS ONE. 2014b; 9:e102097. [PubMed: 25019390]

Key findings

- Zinc is the most abundant transition metal in the mammalian preimplantation embryo
- Labile zinc localizes to cortical regions of cells in the early embryo
- Perturbation of zinc homeostasis severely disrupts embryonic mitotic progression
- Zinc chelation in the embryo alters chromatin and causes global transcription defects

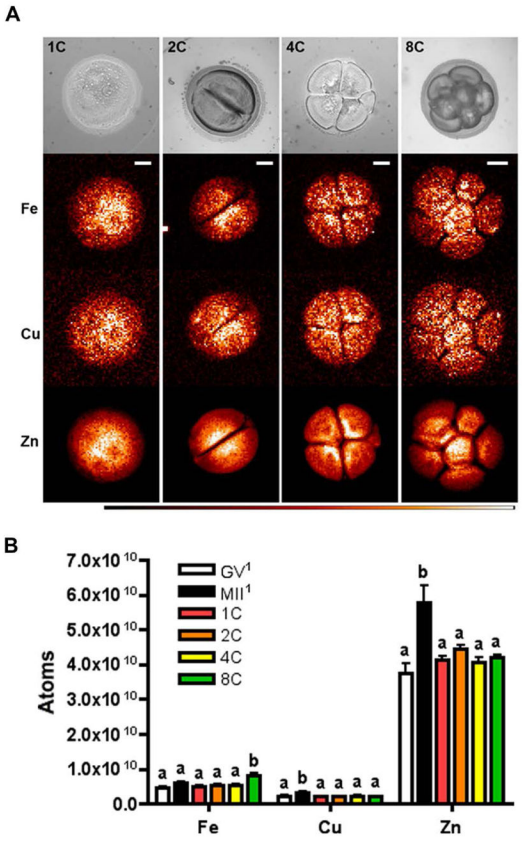

Figure 1. Synchrotron-based X-ray fluorescence microscopy reveals the elemental composition of the preimplantation embryo

(**A**) Preimplantation embryos at the 1- (n = 7), 2- (n = 19), 4- (n = 11) and 8-cell (n = 10) stages were prepared as whole-mount samples for synchrotron-based XFM. Representative bright-field images and the elemental maps for iron, copper and zinc for each stage are shown. White areas represent higher elemental abundance and black areas lower abundance. Scale bar = 20 μm. (**B**) Graph represents mean total elemental content for each embryo stage ± SEM. Letters (a & b) denote statistically significant differences between developmental stages for each element ($p < 0.05$). The superscript[1] denotes data that was previously published in Kim et al., 2010. GV = germinal vesicle stage oocyte, MII = metaphase II stage egg, 1C = one-cell, 2C = two-cell, 4C = four-cell, 8C = eight-cell, Fe = iron, Cu = copper, Zn = zinc.

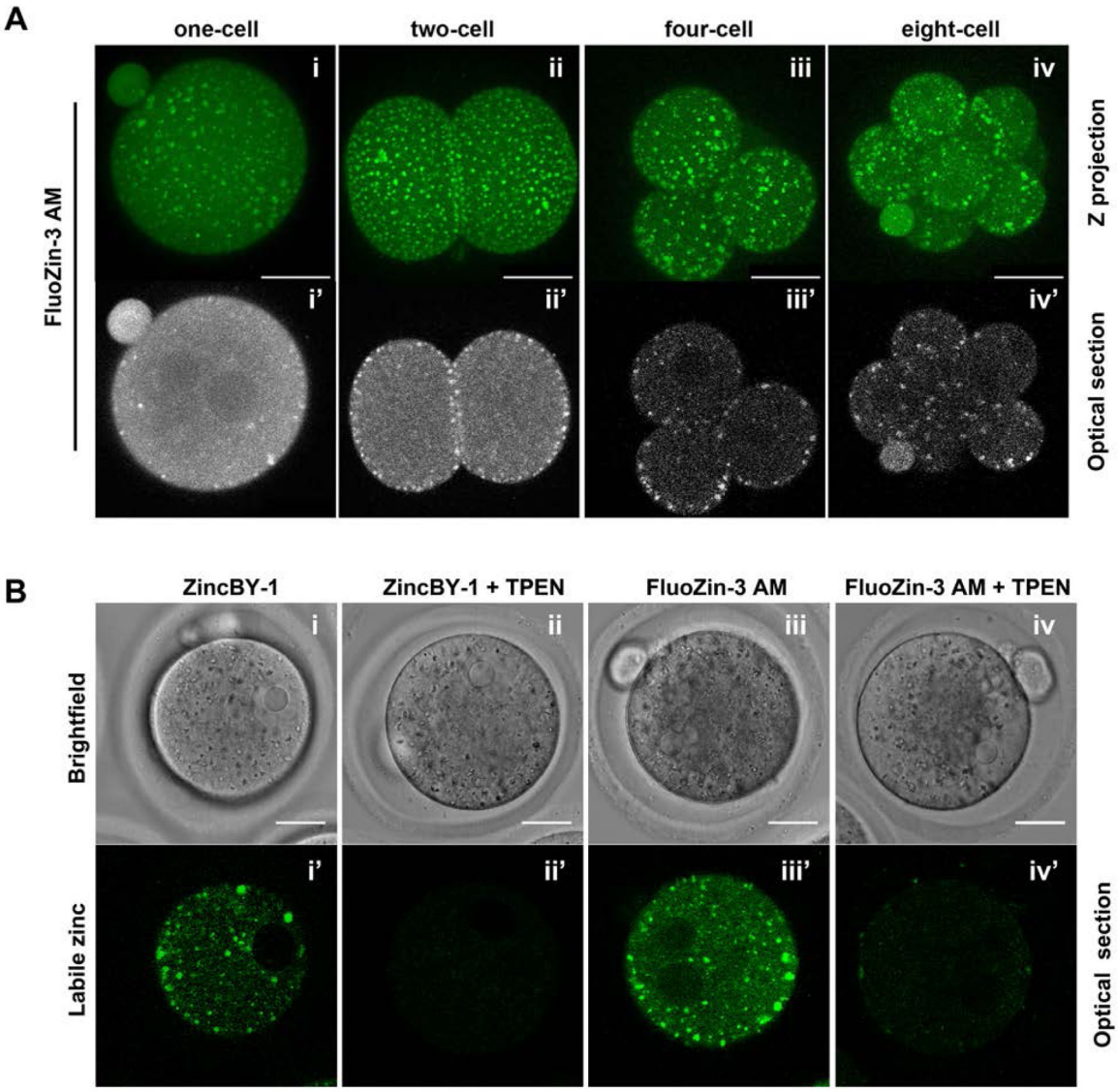

Figure 2. Labile zinc is enriched in cortical vesicles during preimplantation embryo development

(A) Cleavage stage preimplantation embryos were stained for labile zinc using the zinc fluorophore, FluoZin-3 AM, and imaged live. Representative images of both a Z stack-projection (**Ai–iv**) and a single optical section are shown for individual embryos (**Ai′–iv′**). **(B)** As controls for zinc staining specificity, 1C embryos were labeled with two chemically distinct fluorophores, FluoZin-3 AM and ZincBY-1, in the presence or absence of TPEN. Representative brightfield **(Bi–iv)** and fluorescence images of optical sections of individual embryos are shown **(Bi′–iv′).** At least 15 embryos at each developmental stage or with each fluorophore were imaged Scale bars = 25 μm.

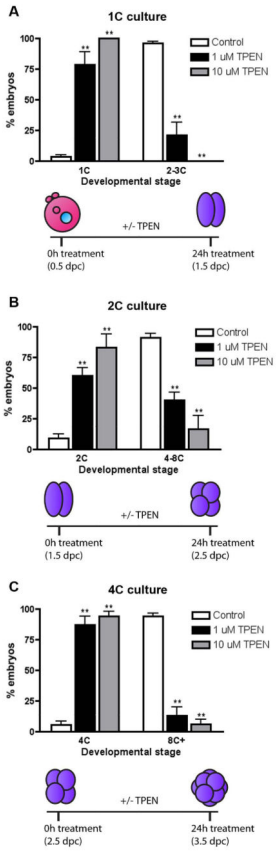

Figure 3. TPEN exposure results in developmental arrest of cleavage stage preimplantation embryos

1C (**A**), 2C **(B)**, and 4C **(C)** embryos were cultured in the presence of 0 μM (white bar), 1 μM (black bar), or 10 μM TPEN (grey bar) for 24 h and developmental progression was scored by morphology. The percentage of embryos at each stage of development per treatment condition was calculated. Experiments were performed in triplicate with a minimum of 20 embryos per group. Results are reported as the mean ± SEM. Asterisks represent statistical significance as compared to control embryos at that particular developmental stage (**$p<0.001$). The schematics below each graph depict the experimental timing and expected developmental stage for control embryos. 1C = one-cell, 2C = two-cell, 4C = four-cell, 8C+ = eight-cell, morula and early blastocyst, dpc = days post coitus.

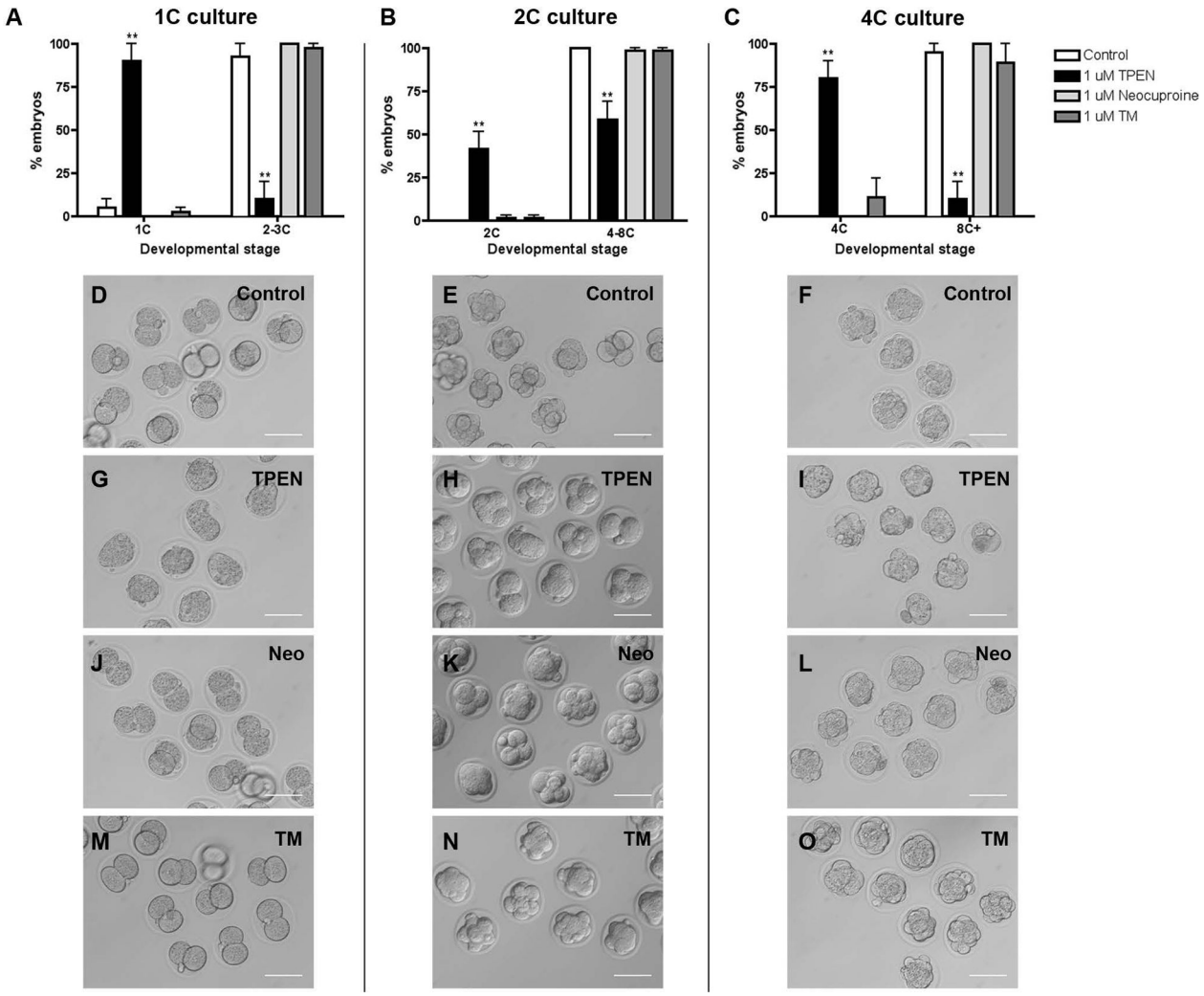

Figure 4. TPEN-induced arrest of preimplantation embryo development is zinc specific

1C, 2C, and 4C embryos were cultured in media alone (control, **D–F**) or with 1 μM TPEN (**G–I**), 1 μM neocuproine (neo, **J–K**) or 1 μM tetrathiomolybdate (TM, **M–O**) for 24 h and developmental progression was scored. (**A–C**) The percentage of embryos at each developmental stage in each treatment condition was calculated. Experiments were performed in duplicate with 7–20 embryos per group. Results are reported as the mean ± SEM. Asterisks represent statistical significance as compared to control embryos at that particular developmental stage (**p<0.001). Representative transmitted light microscopy images of embryos in each treatment group are shown. Scale bars = 80 μm. 1C = one-cell, 2C = two-cell, 4C = four-cell, 8C+ = eight-cell, morula and blastocyst.

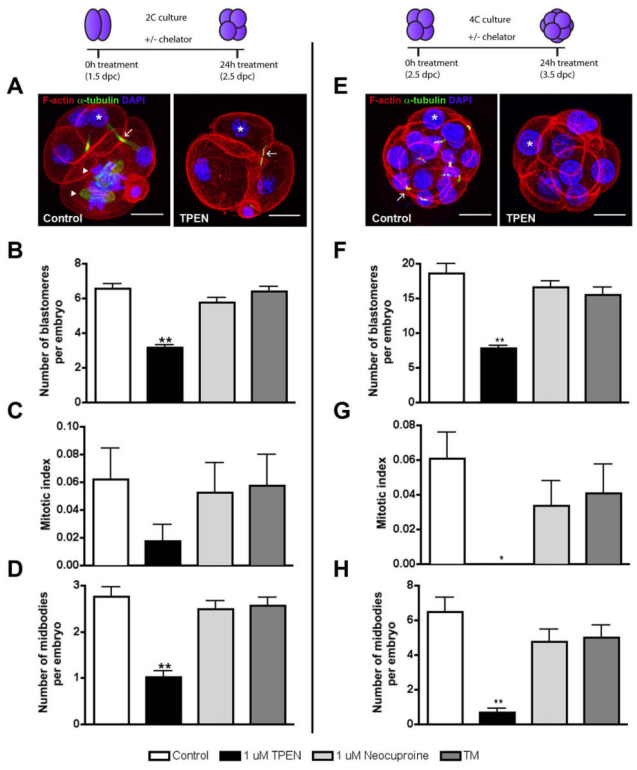

Figure 5. TPEN-induced arrest of preimplantation embryo development is associated with compromised mitotic parameters

2C **(A–D)**, or 4C **(E–H)** embryos cultured in control media or 1 μM TPEN for 24 h were fixed for immunostaining to visualize F-actin (red), α-tubulin (green) and chromatin (blue). Representative images are shown in (**A, E**) and mitotic parameters that were assessed are highlighted. Asterisks denote blastomere nuclei, arrows denote midbodies, and arrowheads denote cells that are undergoing mitotic division. These parameters were used to calculate blastomere number (**B, F**), mitotic index (**C, G**, calculated as number of cells in metaphase or anaphase per total number of blastomeres in embryo), and number of midbodies per embryo (**D,H**). Experiments were performed in duplicate with 7–20 embryos per group. Data in (**B–H**) represent the mean ± SEM. Asterisks represent statistical significance as compared to control embryos (*$p<0.01$, **$p<0.001$). Schematics at the top of the figure depict experimental timing and expected developmental stage for control embryos. Scale bar = 20 μM.

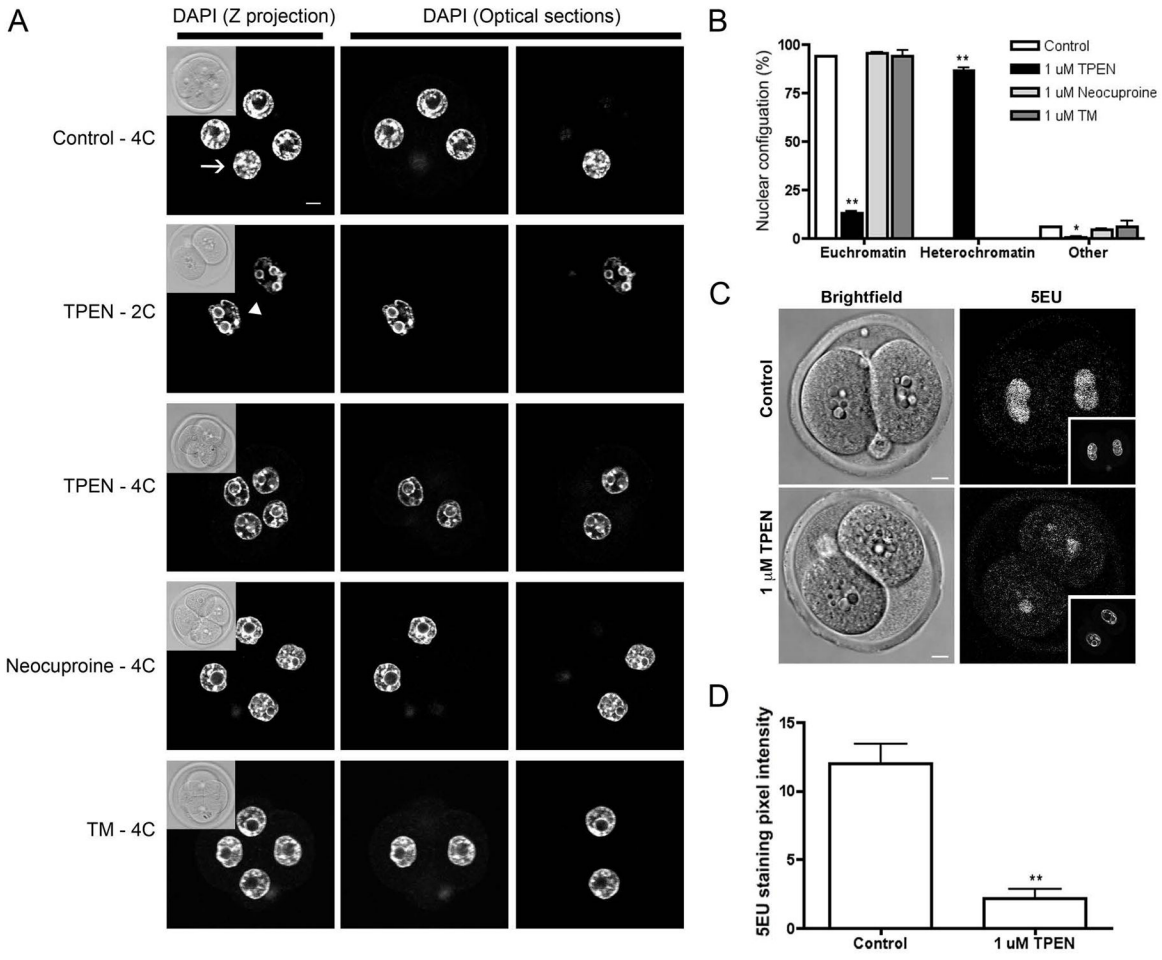

Figure 6. TPEN exposure results in chromatin and global transcription alterations in the preimplantation embryo

(**A**) 2C embryos were cultured for 24 h in control media or media containing 1 μM TPEN, 1 μM neocuproine, or 1 μM tetrathiomolybdate (TM) for 24 h and then fixed and immunostained to visualize chromatin morphology with DAPI. For each treatment group, the Z-projection image is shown alongside optical sections where the nuclei were visible in each individual blastomere of an embryo. Insets represent brightfield images. Arrows highlight blastomeres containing DNA in a euchromatin configuration, arrowheads highlight blastomeres containing DNA with a prominent heterochromatin. (**B**) The percentage of embryos with euchromatin and heterchromatin were quantified. Experiments were performed in duplicate with 7–20 embryos per group. Data represent the mean ± SEM. Asterisks represent statistical significance as compared to control embryos (*$p<0.05$, **$p<0.001$). (**C**) Embryos were cultured in the presence or absence of 1 μM TPEN for 24 h and processed for 5-ethynyl uridine (5EU) incorporation. Representative brightfield images and images of 5EU incorporation are shown for embryos in each treatment group. Insets show the nuclear area as defined by DAPI staining. (**D**) Quantification of global transcriptional activity according to the mean intensity of 5EU incorporation within the nuclear area. Experiments were performed in duplicate with 12–15 embryos per group.

Results represent the mean ± SEM. Asterisks represent statistical significance as compared to control embryos in that developmental stage (**p<0.001). Scale bar = 10 μM.

Table 1

Summary of numerical values for total iron, copper and zinc levels in the preimplantation embryo represented as the number of atoms per embryo as determined by synchrotron-based X-ray fluorescence microscopy.

	atoms × 10^9			
	Fe	**Cu**	**Zn**	**Total embryo volume (μm^3)**
One-cell	**4.9 ± 0.3**	**2.1 ± 0.2**	**41.3 ± 1.3**	
	44 μM	19 μM	370 μM	185,559
Two-cell	**5.5 ± 0.2**	**2.2 ± 0.1**	**44.3 ± 1.1**	
	40. μM	16 μM	320 μM	230,385
Four-cell	**5.5 ± 0.2**	**2.3 ± 0.2**	**39.0 ± 1.6**	
	48 μM	20 μM	340 μM	192,325
Eight-cell	**8.2 ± 0.5**	**2.2 ± 0.1**	**42.2 ± 7.1**	
	79 μM	21 μM	404 μM	173,324

Values in bold represent number of atoms × 10^9 ± SEM. Values in shaded gray boxes represent approximate molarities (μMF) of total iron, copper, and zinc levels as calculated based on atom number per embryo and previously published embryo volumes (Aiken et al., 2004). Fe = iron, Cu = copper, Zn = zinc.

Aiken, C.E., Swoboda, P.P., Skepper, J.N., Johnson, M.H., 2004. The direct measurement of embryogenic volume and nucleo-cytoplasmic ratio during mouse pre-implantation development. Reproduction 128, 527–535.

Table 2

Summary of numerical values for percentages of embryos at each stage of development in the presence of metal chelators.

		Total no. of embryos	Percent embryos arrested ± SEM[1]	Percent embryos progressed ± SEM[2]
1C culture	Control	35	5.0 ± 5.0	95.0 ± 5.0
	TPEN	35	90.0 ± 10.0**	10.0 ± 10.0**
	Neocuproine	35	0.0 ± 0.0	100.0 ± 0.0
	TM	34	2.5 ± 2.5	97.5 ± 2.5
2C culture	Control	62	0.0 ± 0.0	100.0 ± 0.0
	TPEN	92	41.4 ± 10.2**	58.6 ± 10.2**
	Neocuproine	92	1.6 ± 1.6	98.4 ± 1.6
	TM	65	1.6 ± 1.6	98.4 ± 1.6
4C culture	Control	31	0.0 ± 0.0	100.0 ± 0.0
	TPEN	30	88.9 ± 11.1**	11.1 ± 11.1**
	Neocuproine	29	0.0 ± 0.0	0.0 ± 0.0
	TM	30	11.1 ± 11.1	88.9 ± 11.1

All embryos were cultured for 24 h. 1C = one-cell, 2C = two-cell, 4C = four-cell, TM = tetrathiomolybdate. Asterisks represent statistical significance as compared to control embryos

** $p<0.001$

[1] Embryos were scored as arrested if, after 24h of culture, they were one-cell embryos for the 1C culture, two-cell embryos for the 2C culture, and four-cell embryos for the 4C culture.

[2] Embryos were scored as progressed if, after 24h of culture, they were two-to-three-cell embryos for the 1C culture, four-to-eight-cell embryos for the 2C culture, and eight-cell or beyond embryos for the 4C culture.

Table 3

Summary of numerical values for mitotic parameters in cleavage stage embryos cultured in the presence of metal chelators.

		Total no. of embryos	No. of blastomeres per embryo ± SEM	Mitotic index ± SEM	No. of midbodies per embryo ± SEM
2C culture	Control	42	6.5 ± 0.30	6.2 ± 2.3	2.8 0.21
	TPEN	38	3.2 ± 0.14**	1.8 ± 1.2	1.0 ± 0.13**
	Neocuproine	45	5.8 ± 0.29	5.1 ± 2.1	2.5 ± 0.19
	TM	57	6.4 ± 0.26	5.8 ± 2.2	2.6 ± 0.18
4C culture	Control	17	19 ± 1.3	6.1 ± 1.5	6.5 ± 0.87
	TPEN	18	7.8 ± 0.48**	0.0 ± 0.0*	0.67 ± 0.27**
	Neocuproine	17	17 ± 0.88	3.4 ± 1.4	4.8 ± 0.73
	TM	16	16 ± 1.1	4.1 ± 1.7	5.0 ± 0.73

All embryos were cultured for 24 h. Mitotic index = number of cells in metaphase or anaphase divided by total number of blastomeres in embryo, 2C = two-cell, 4C = four-cell, TM = tetrathiomolybdate. Asterisks represent statistical significance as compared to control embryos

* $p<0.01$

** $p<0.001$

Table 4

Summary of numerical values for percentage of blastomeres with euchromatin and heterochromatin configurations in embryos cultured in the presence of metal chelators.

	Total no. of blastomeres (n)	Percent of blastomeres with euchromatin ± SEM%	Percent of blastomeres with heterochromatin ± SEM%	Percent of blastomeres in mitosis ± SEM%
Control	273	94.1 ± 0.064	0.0 ± 0.0	5.9 ± 0.064
TPEN	150	13.2 ± 0.90**	86.2 ± 1.5**	0.59 ± 0.59*
Neocuproine	248	95.2 ± 0.38	0.0 ± 0.0	4.8 ± 0.38
TM	373	93.9 ± 2.7	0.0 ± 0.0	6.1 ± 2.7

All embryos were cultured for 24 h. TM = tetrathiomolybdate. Asterisks represent statistical significance as compared to control embryos

* $p<0.01$

** $p<0.001$